Available online at www.sciencedirect.com

SciVerse ScienceDirect

Geochimica et Cosmochimica Acta 109 (2013) 38–50

Geochimica et Cosmochimica Acta

www.elsevier.com/locate/gca

Small molecule – Silica interactions in porous silica structures

Di Wu, Alexandra Navrotsky *

Peter A. Rock Thermochemistry Laboratory and NEAT ORU (Nanomaterials in the Environment, Agriculture, and Technology Organized Research Unit), University of California, Davis, One Shields Avenue, Davis, CA 95616, United States

Received 12 August 2012; accepted in revised form 29 January 2013; available online 8 February 2013

Abstract

A series of porous silica frameworks with different pore sizes (SSZ-59, MCM-41 and SBA-15) was studied by immersion calorimetry in various solutions (water, ethanol, triethylamine, NaCl brine and Na_2CO_3/$NaHCO_3$ buffer) at 25 °C to determine the interaction energies between inorganic silica frameworks and various small molecules which may be of importance in the context of CO_2 sequestration, carbonate mineralization, and environmental remediation. The enthalpies of immersion for the calcined porous silica samples range from −0.7 to −9.6 kJ per mole of SiO_2 in water, −3.4 to −10.5 kJ per mole of SiO_2 in ethanol, −5.7 to −15.1 kJ per mole of SiO_2 in triethylamine, −1.5 to −11.4 kJ per mole of SiO_2 in NaCl brine (1 M) and −0.5 to −8.0 kJ per mole of SiO_2 in a Na_2CO_3/$NaHCO_3$ buffer solution (1 M). The enthalpies of interaction between porous silicas and water, ethanol and triethylamine vary from −0.3 to −2.3 kJ per mole of H_2O, from −49.1 to −62.5 kJ per mole of ethanol and from −65.5 to −95.6 kJ per mole of triethylamine. The enthalpies of interaction suggest that guest–host interactions in silica-based porous media are governed both by pore size and concentration of surface hydroxyl groups. The generally hydrophobic surfaces of porous silica materials bond more strongly to organic molecules (ethanol and triethylamine) than to aqueous solutions and the energetics of such functionalized organic – rich silica surfaces could play a significant role in geologic CO_2 sequestration, enhanced oil recovery, and geochemistry in low-temperature diagenetic and sedimentary environments.

1. INTRODUCTION

Large sedimentary basins below depths of 800–1000 m, having interlayered sedimentary rocks with large pore space, have been explored as potential storage options for supercritical CO_2 ($scCO_2$) (Bachu and Stewart, 2002; Benson and Cole, 2008). The impermeable silica-rich shale or fine-grained mudstone serves as seals or caprock to trap the CO_2 underground. Depleted oil and gas reservoirs, saline aquifers, and coal beds are also possible options for geological CO_2 sequestration (Li et al., 2006; Benson and Cole, 2008). Reservoir formations are generally made up of sandstones, shales and sometimes feldspars and/or volcanic rock fragments. These form a porous structure by connecting gaps between these grains (Li et al., 2006). Quartz, clay (mainly smectite and chlorite), dolomite, gypsum, anhydrite, and halite are the common minerals found in these shales and sandstones.

CO_2 sequestration in geological formations is a complex process that involves various geochemical reactions. The principal mechanisms are initial trapping of CO_2 below impermeable caprocks (structural/hydrodynamic trapping), adsorption or confinement of CO_2 in porous structures and at mineral surfaces in the storage sites (capillary/residual phase trapping), dissolution of CO_2 in fluids present in the formation (solubility trapping), and finally carbonate mineral formation (mineral trapping) (Benson and Cole, 2008). The nucleation and growth of carbonate phases in nanoporous or mesoporous structures could vary with reservoir temperature, pressure and pH conditions. Multiphase flow – reactive chemical transport models and geochemical models have been used to calculate thermodynamic, kinetic, and reaction paths for geologic sequestration (Schnaar and Digiulio, 2009; Cole et al., 2010; Wurdemann et al., 2010). These modeling studies need thermodynamic data of minerals and solutions, including effects of confinement in small (nanosized) pores, to constrain pos-

* Corresponding author.
E-mail address: anavrotsky@ucdavis.edu (A. Navrotsky).

0016-7037/$ - see front matter © 2013 Elsevier Ltd. All rights reserved.
http://dx.doi.org/10.1016/j.gca.2013.01.038

sible geochemical reactions, including $scCO_2$ solubility, aqueous complexation, redox reactions, mineral dissolution, and precipitation of new secondary carbonate, silicate, oxide, and hydroxide minerals (Marini, 2007).

Organic–inorganic interactions on mineral surfaces play crucial roles in geological processes, particularly in environments where one can expect significant concentrations of a complex mixture of organic compounds (Dove et al., 2003; Weiner and Dove, 2003; Benson and Cole, 2008). Nevertheless, the molecular interactions that may affect mineral precipitation on organic–inorganic interfaces, especially in the deep earth reservoir, are still poorly understood. In natural environments, mineral surfaces and pores are generally covered by aqueous solutions and/or organic constituents from both living and dead organisms. Consequently, before contacting the mineral surfaces, the CO_2 and carbonate species introduced in sequestration must interact and compete with molecules already adsorbed on the mineral surfaces or confined in the pores (Bertier et al., 2006; Kharaka et al., 2006a,b; Assayag et al., 2008). Hence, thermochemical data for the interaction between inorganic frameworks and various guests (small organic molecules and aqueous solutions) are important to properly model CO_2 sequestration under geologic conditions, oil recovery, and geochemical processes at relatively low temperature.

In our earlier studies, various calorimetric techniques have been designed to investigate small molecule–porous media interactions. Piccione et al. (2002) studied the interactions of four different zeolites with several quaternary ammonium structure directing agents using hydrofluoric acid (HF) solution calorimetry. The measured enthalpies of interaction were −1.0 to −6.0 kJ per mole of SiO_2. Measurements for mesoporous silica phases (Trofymluk et al., 2012) showed similar but slightly stronger interactions. Measurements of the hydration enthalpies of a series of cation – exchanged aluminosilicate zeolite beta by Sun et al. (Sun et al., 2006, 2007; Sun and Navrotsky, 2008a) suggest that water is held more tightly in more aluminum – rich systems than in high Si:Al ratio zeolitic frameworks. The interaction energetics of water with ion – exchanged gallosilicate zeolites were found to be similar to those in aluminosilicates (Sun and Navrotsky, 2008b; Zhou et al., 2011).

In the present study, we selected silica with different well – controlled pore sizes as a simple model for geological silica-rich systems with small pores. We picked zeolite SSZ-59 and mesoporous silica MCM-41 and SBA-15 to study the interaction of porous silica structures with small organic molecules and with different aqueous solutions, including water, ethanol (99.5+% purity, Sigma–Aldrich), triethylamine (99.5+% purity, Sigma–Aldrich), NaCl brine and Na_2CO_3/$NaHCO_3$ buffer. MCM-41 and SBA-15 are two families of mesoporous silicas having amorphous silica walls separating periodic two dimensional arrays of hexagonally-arranged pores with a narrow pore size distribution. Their tunable pore size, in the range 2–30 nm, scarce defect sites, and a relatively hydrophobic surface make them potentially suitable materials for gas separation, drug delivery and catalysis (Glinka et al., 1996; Corma, 1997; Zhao et al., 1998; Kruk et al., 2000; Hoang et al., 2005). Even though SBA-15 has a similar symmetry and structure as MCM-41, the microstructure of its pores is significantly different. It has a significant amount of microporosity interconnecting its mesopores. Such microporosity is not present in MCM-41 (Ryoo et al., 2000; Trofymluk et al., 2005). SSZ-59 is a synthetic 14-membered ring pure silica zeolite with a pore diameter of 0.8 nm (Burton et al., 2003, 2004).

These three silica frameworks provide ordered nanopore systems as idealized analogues to more complex porous rocks. The enthalpies of immersing these calcined (anhydrous) porous silicas in water, ethanol, triethylamine and two aqueous solutions (1 M NaCl brine and 1 M Na_2CO_3/$NaHCO_3$ buffer) were measured at room temperature. The water, brine, and buffer solution are obviously relevant to the sequestration environment. The ethanol and triethylamine were chosen as model polar molecules showing potentially stronger interactions than water with mineral surfaces. Because they can be used as pure liquids, one can focus on their interaction with silica rather than on a competition between the interaction of the organic molecule and water. Thus, this is a good starting point for the study of pore size effects and sets the stage for investigations of more complex systems, with many organics in dilute aqueous solution, encountered in natural environments. The enthalpy of absorbing the liquid into the initially empty pores provides a measure of the strength of interaction between the silica and the guest molecules. These results are discussed in terms of interactions potentially important to the CO_2 sequestration environment.

2. EXPERIMENTAL METHODS

2.1. Materials

SSZ-59 was prepared at the Chevron Energy and Technology Center, Richmond, California and its synthesis and characterizations are described elsewhere (Burton et al., 2003, 2004).

MCM-41 was synthesized at room temperature and ambient pressure according to the method reported by Gallis and Landry (1997) using *n*-hexadecyltrimethylammonium bromide (CTAB, 99+% purity, Alfa Aesar) as structure directing agent (SDA). NaOH (5.0 g, 2 M in H_2O) was mixed with an aqueous solution of CTAB (39.2 g H_2O/0.8 g CTAB) and the mixture was stirred until CTAB was totally dissolved. Subsequently, 3.85 g of tetraethoxysilane (TEOS, 99+% purity, Sigma–Aldrich) was added to the clear solution of CTAB as a silicate source. After 3 h of reaction under stirring, the precipitate was collected, filtered and washed with deionized water. The MCM-41 samples synthesized by this method have uniform cylindrical mesopores around 2 nm in diameter.

SBA-15 samples were synthesized hydrothermally in an autoclave using BASF Pluronic P123, (a triblock poly(ethylene oxide) (PEO) and poly(propylene oxide) (PPO)-based copolymer system, $(PEO)_{20}(PPO)_{70}(PEO)_{20}$, with a molecular weight of 5800 g/mol) as structure directing agent (SDA) (Zhao et al., 1998; Fusco et al., 2006). In a typical synthesis, 4.0 g of Pluronic P123 was dissolved in 30.0 g of water and 120.0 g of 2 M HCl solution under stirring.

Subsequently, 8.5 g TEOS was added to the clear solution. The autoclave was transferred into an oil bath, maintained at 35 °C for 12 h and then another 48 h at 60 °C. The mixture was then aged at 120 °C for 48 h under static condition in a Teflon-lined autoclave. The solid product was triple washed with deionized water and dried in air at room temperature. The SBA-15 synthesized by this method has uniform pore sizes from 5 to 10 nm, it can be expanded up to 30 nm by an organic co-solvent such as 1,3,5-trimethylbenzene (TMB, 99+% purity, Alfa Aesar). In this work, the SBA-15 samples with pores larger than 10 nm were made using TMB.

All synthesized porous silica samples were calcined in a Lindberg/blue tube furnace by heating at 1 °C/min from room temperature to 500 °C. The samples were calcined at this temperature for 8 h under N_2 and another 8 h under O_2. The silica furnace tube was then sealed under dry nitrogen, the furnace cooled, and the samples transferred into a nitrogen-filled glove box to prevent adsorption of moisture. Prior to each calorimetric measurement, 3–7 mg sample pellets were hand-pressed and sealed in small plastic vials in the glove box, then transferred to the calorimeter. Exposure to laboratory air was limited to about 10 s.

2.2. Characterization

The powder X-ray diffraction (XRD) patterns of all porous silica samples were collected using an Inel X-ray diffractometer (XRG 3000) operated at 30 kV and 30 mA, with Cu Kα radiation ($\lambda = 0.15406$ nm) with a Ni – filter. Data were acquired in the 2θ range 0.5–50°, where diffraction peaks from the periodic pore arrangement can be seen and are indicative of a well ordered pore structure. At higher angles, because the mesoporous silica walls are amorphous, no further diffraction peaks are seen.

A Micromeritics ASAP 2020 instrument was employed to measure the adsorption/desorption isotherms of nitrogen on all porous silica samples at −196 °C. Prior to isotherm analyses, all samples were degassed at 200 °C overnight to maximize H_2O removal. The Dubinin–Astakhov equation (Astakhov and Dubinin, 1971) and the Barrett–Joyner–Halenda (BJH) method (Barrett et al., 1951; Joyner et al., 1951) were used to calculate the pore properties of microporous and mesoporous silicas, respectively.

2.3. Immersion calorimetry

The enthalpies of immersion of the porous silicas in various solutions (water, ethanol, triethylamine, 1 M NaCl brine and 1 M Na_2CO_3/$NaHCO_3$ buffer solution) were determined at 25 ± 0.5 °C using a Setaram C-80 twin microcalorimeter equipped with a custom – made dropping tube. Loosely hand-pressed pellets of porous silica samples weighing between 5 and 10 mg were dropped from room temperature (22 ± 0.5 °C) into a solution maintained at 25 °C. In our measurement, the heat effect due to this temperature difference is less than the experimental error of the measurements and can be neglected. The drop generates the heat effect associated with the interaction of the anhydrous silica with solution. The normal return of the calorimetric signal to its initial value (baseline) indicated the rapid completion of reaction. Typically, a measurement takes 45–90 min. The reproducibility of these measurements is documented as error bars in the calorimetric data figures and as errors (2 standard deviations of the mean) in Tables.

2.4. Thermogravimetric analysis (TG) and differential scanning calorimetry (DSC)

TG–DSC experiments were performed using a Netzsch STA 449 system (Netzsch GmbH, Selb, Germany) to investigate the thermal behavior of each silica sample containing the adsorbed solution and to obtain the amount of adsorbed solution. After each immersion calorimetry experiment, the solid sample was collected and dried at room temperature until the sample mass did not change. Subsequently, 10–20 mg samples were hand-pressed into pellets, placed into a Pt crucible and heated from 30 to 800 °C in argon at 10 °C/min. Buoyancy correction was performed for all experiments by running TG–DSC on empty Pt crucibles under the same experimental conditions. Calcined porous silicas were also heated similarly to estimate the concentration of hydroxyl groups on their surfaces (Mueller et al., 2003).

2.5. Fourier transform infrared spectroscopy (FTIR) for evolved gas analysis (EGA)

The gases evolved during thermal analysis were analyzed by a FTIR spectrometer (Bruker Equinox 55), directly coupled to the Netzsch STA 449 system by a transfer line kept at 150 °C. FTIR spectra of evolved gases were scanned from 400 to 4000 cm^{-1} at a resolution of 4 cm^{-1}.

3. RESULTS

3.1. Structure

The powder X-ray diffraction patterns of mesoporous silica samples confirmed that all samples were two dimensional hexagonal ordered structures. The XRD patterns (Fig. 1) after calcination (500 °C) and TG–DSC (800 °C) indicate that all porous silica samples (SSZ-59, MCM-41 and SBA-15) maintained their structure without significant degradation or phase transformation.

Nitrogen adsorption/desorption isotherms and pore size distribution curves of calcined mesoporous silica samples are presented in Fig. 2. A type I isotherm is observed for nitrogen adsorption on microporous silica (zeolite SSZ-59) whose pore size is not significantly larger than the molecular diameter of nitrogen. The complete filling of its micropores only needs a single adsorbed nitrogen layer. This also explains why the desorption and adsorption curves of SSZ-59 follow the same path. All the mesoporous silicas (MCM-41 and SBA-15) present typical type IV adsorption curves with sharp rising hysteresis loops, indicating that the desorption is distinct from the adsorption process due to nitrogen condensation. These hysteresis loops are signature evidence of mesoporosity in materials (Ball and Evans, 1989). The measured properties are listed

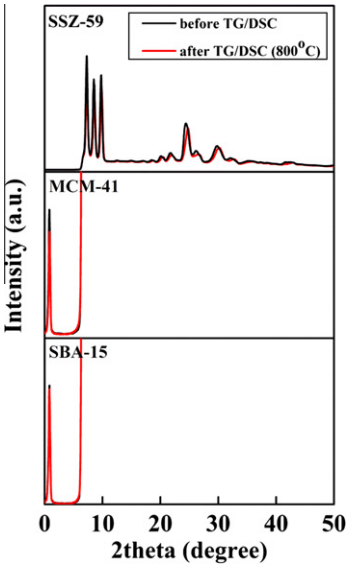

Fig. 1. Powder X-ray diffraction patterns of all porous silica phases in this work (before and after calcination at 800 °C).

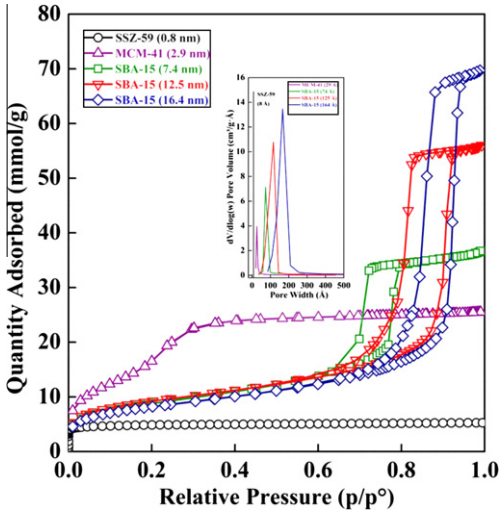

Fig. 2. Nitrogen adsorption/desorption isotherms and pore size distribution curves of all porous silicas used in this work.

in Table 1. All analyzed porous silica samples have uniform pore structure and narrow pore size distribution.

3.2. Immersion calorimetry

The enthalpies of immersion of porous silica in various solutions were measured at 25 °C. The immersion process is represented by the equation:

$$SiO_2\,(\text{calcined}) + \text{solution} \rightarrow SiO_2\,(\text{immersed}) \quad \Delta H_{imm}(25\,^{\circ}C) \tag{1}$$

The final state of this experiment is a sample that has absorbed the solution into its pores and is in contact with the solution.

Two experiments were designed to confirm that the immersion calorimetry experiments (45–90 min) were carried out long enough to attain equilibrium (or at least steady state on a timescale of days) with respect to the amount of absorbed solution. In the first experiment, a loosely hand-pressed pellet of porous silica sample (SBA-15, 12.5 nm) was dropped from room temperature (22 ± 0.5 °C) into ethanol maintained at 25 °C in the calorimeter. The calorimetric signal of this drop was recorded for 4 days. There was no detectable calorimetric signal after the sharp, well resolved peak recorded in the first 90 min of the drop. The extremely stable baseline signal, identical to that before the experiment, shows that there is no significant additional heat generated at long times (up to 4 days in this experiment). In the second test, two SBA-15 (12.5 nm) pellets were hand-pressed. They were then dropped: the first into the calorimeter containing ethanol, the second into a glass vial of ethanol kept at room temperature. The first pellet was taken out for equilibration in air after the calorimetric signal returned to the initial baseline (about 90 min). The second pellet was kept in the glass vial for 4 days to maximize pore – filling before equilibration in ambient air. When the weight of the post – immersion silica was stable (the sample weight did not change by more than 0.5 wt.% during 48 h), each pellet was subjected to thermogravimetric analysis. TG analysis showed total weight loss (−7.04% (first pellet) and 6.78% (second pellet)). The variation is within the experimental error of the methodology. Thus, we conclude that no additional pore – filling is seen in the 4-day experiment. In addition, if any molecules from inside the pores or on the particle surfaces are easily removed during air drying, those molecules would have weak interactions with the framework and thus not contribute significantly to the immersion enthalpy. Thus, attributing the immersion enthalpy to the molecules which remain associated with the silica matrix after air drying focuses on those molecules that are strongly bound and have enthalpies significantly different from those of molecules in the solution. Moreover, X-ray diffraction patterns before and after immersion calorimetry experiments also confirmed that the silicas maintained their structures.

The host–guest interactions in these mesoporous and microporous silicas are chemically and structurally complex, as are the interactions among the guest molecules themselves. The internal surfaces may not be uniformly coated with guest molecules, and not all guest molecules are bound to a surface. Thus, we do not believe that calorimetric measurements should be normalized to the surface area of the solids. Alternatively, in our analysis and interpretation of enthalpies of immersion and interaction, we present thermochemical data both per mole of solid and per mole of liquid, the latter focusing on the number of guest molecules inside the pores.

The enthalpies of immersion are shown in Table 2. Fig. 3 shows the enthalpies of immersion of porous silica in water, ethanol and triethylamine as a function of pore size. The enthalpies of immersion in triethylamine are more exothermic than those in ethanol and water. They vary from −5.7 (SSZ-59) to −15.1 (MCM-41) kJ/mol SiO_2. Immersion enthalpies in water are least exothermic and range from −0.7 (SSZ-59) to −9.6 (MCM-41) kJ/mol SiO_2. For each solution, the silica zeolite sample SSZ-59 shows the least

Table 1
Properties of porous silica samples studied.

Sample ID	Pore size (nm)	Pore volume (cm^3/g)	Micropore volume (cm^3/g)	Specific surface area (m^2/g)	Calculated concentration of OH (molecules/nm^2)
SSZ-59	0.8[a]	0.13[a]	0.13[a]	440.3	0.8
MCM-41	2.9	0.52	N/A	1403.9	1
SBA-15_1	7.4	1.30	0.03	710.9	3.3
SBA-15_2	12.5	1.92	0.05	740.4	4.8
SBA-15_3	16.4	2.44	0.04	662.5	5.2

[a] Values reported by Burton et al. determined by the *t*-plot method using density functional theory (DFT) analysis (Burton et al., 2003).

exothermic enthalpy of immersion per mole of SiO_2 and MCM-41 gives the most exothermic value. The samples with primary pore size 2.9 nm (MCM-41) to 16.4 nm (SBA-15) exhibit a roughly linear correlation of immersion enthalpy with pore size. Mesoporous silica samples with larger pores tend to generate less exothermic heat effects than those with smaller pore size.

To better simulate the geologic carbonate mineralization environment, immersion enthalpies of porous silicas were also measured in two concentrated aqueous solutions, 1 M NaCl brine and 1 M Na_2CO_3/$NaHCO_3$ buffer (see Table 2 and Fig. 4). Immersion enthalpies in brine are most exothermic and range from −1.5 (SSZ-59) to −11.4 (MCM-41) kJ/mol SiO_2. For SSZ-59 and MCM-41, the immersion enthalpies in the Na_2CO_3/$NaHCO_3$ buffer solution show the least exothermic values. The enthalpies of immersion of all porous silicas in aqueous solutions are less exothermic than those in triethylamine.

3.3. Thermal analysis

After immersion calorimetry, the porous silica samples were collected and equilibrated at room temperature until there was no weight loss. TG–DSC analyses were then carried out on these "solution-absorbed/confined" porous silica samples. Fig. 5 shows the TG–DSC traces of SSZ-59, MCM-41 and SBA-15 with absorbed/confined water, ethanol or triethylamine molecules. A positive DSC signal indicates an exothermic heat effect (releasing energy in the form of heat). All water-containing porous silica samples show one-step weight loss slightly above 100 °C with large endothermic DSC peaks. The FTIR spectra (not shown) of the gases evolved at this temperature range confirm the removal of H_2O. Similar H_2O removal between 100 and 150 °C was also observed in aluminosilicate and gallosilicate zeolites (Sun et al., 2006, 2007; Sun and Navrotsky, 2008a,b; Zhou et al., 2011).

The thermograms for silica containing ethanol or triethylamine exhibit two-step desorption. The various porous silica samples with ethanol show different thermal behavior. The first endothermic peak at about 125 °C, due to loss of ethanol is common to all samples. This temperature is significantly higher than the boiling point of ethanol (78.4 °C), supporting energetically favorable confinement. Ethanol-containing MCM-41 shows a second endothermic peak slightly above 500 °C, associated with the second step of weight loss on the TG curve. Desorption and partial decomposition of tightly absorbed ethanol molecules is responsible for this heat effect, as confirmed by FTIR (not shown) which indicates the evolution of various carbon-containing fragments near 500 °C. The DSC trace of ethanol-containing SSZ-59 and SBA-15 show well resolved exothermic peaks at 500 °C and are very different from that of MCM-41. The TG curve of ethanol-containing SBA-15 has a distinct second weight loss step, similar to that of MCM-41, whereas there is no step-like slope change on the TG trace of ethanol-containing SSZ-59. Ethanol could not be removed from mesoporous silica frameworks even after heating at 120 °C under vacuum. Our recent FTIR and solid-state MAS NMR results, to be published separately, provide further evidence that ethanol interacts strongly with mesoporous silicas.

The DSC traces of triethylamine-containing porous silicas show two endothermic peaks. The first broad peak between 30 and 300 °C indicates removal of loosely bound triethylamine on the surfaces or in the silica mesopores. The second endothermic peaks for MCM-41 and SBA-15 appear slightly above 300 °C and almost merge with the first peak. In contrast, the second endothermic peak of triethylamine-containing SSZ-59 at about 420 °C is well separated from the first peak. These results suggest stronger interactions between microporous zeolite SSZ-59 and triethylamine than between mesoporous silicas (MCM-41 and SBA-15) and triethylamine. The thermogravimetric data are summarized in Tables 3a and 3b.

3.4. Enthalpy of interaction

The interaction enthalpies of porous silicas with water, ethanol and triethylamine versus pore size are plotted in Fig. 6a and b. Enthalpy of interaction is defined here as the immersion enthalpy per mole of absorbed/confined molecules (from TG–DSC analyses). Table 4 shows the interaction enthalpies of porous silicas with water, ethanol and triethylamine calculated using weight loss data from TG–DSC (Table 3a). Porous silica with pore size from 0.8 to 16.4 nm has interaction enthalpies from −0.3 to −2.3 kJ per mole of H_2O, −49.1 to −62.5 kJ per mole of ethanol and −65.5 to −95.6 kJ per mole of triethylamine. The enthalpies of interaction of SSZ-59 with both ethanol and triethylamine are more exothermic than that of MCM-41 (see Fig. 6a). In the mesoporous region, the interaction enthalpies of porous silicas with ethanol and triethylamine tend to be more exothermic as the pore size

increases. Considering only the primary pores, this weak linear correlation contradicts the trend from SSZ-59 to MCM-41. These results suggest that interaction enthalpy of porous silica with various solutions is related to the pore structures as well as the pore size of the silica hosts.

4. DISCUSSION

4.1. Porosity and guest–host interactions

One of the most appropriate measures of molecular size is the critical molecular diameter which is defined as the diameter of the smallest cylinder that can just circumscribe the molecule in its equilibrium configuration (Ruthven, 2011). Zeolite SSZ-59 has elliptical 14-member ring micropores with 0.85 × 0.65 nm dimensions (Burton et al., 2003, 2004), which are nearly the same size as the largest molecule, triethyamine (critical diameter 0.78 nm), (deCarvalho et al., 1996) and larger than the critical diameter of ethanol (0.44 nm), (Lalik et al., 2006). The confinement of ethanol and triethylamine molecules in micropores of SSZ-59 results in strong exothermic interaction enthalpies, in part because the molecules can probably interact simultaneously with a number of locations on the pore walls because they are a "tight fit" into the pores.

The mesoporous silica phases MCM-41 and SBA-15 have hexagonal symmetry (*p6mm*) (Zhao et al., 1998), with honeycomb arrays of non-intersecting primary channels (Rathousky et al., 1994; Glinka et al., 1996). SBA-15 also contains a significant number of micropores (0.5–1.5 nm), (Galarneau et al., 2003; Pollock et al., 2011) interconnecting the primary mesopore channels (Kruk et al., 2000; Ryoo et al., 2000; Che et al., 2003; Hoang et al., 2005; Trofymluk et al., 2005). The use of the Pluronic P123 polymer as structure directing agent imparts this unique microstructure to SBA-15 (Ryoo et al., 2000; Trofymluk et al., 2005). In SBA-15, the presence significant microporosity may provide strong overall steric effects to guest molecules. A previous study (Hoang et al., 2005) suggests that SBA-15 samples having high microporosity show high activation energies for diffusion and relatively low diffusivities for *n*-heptane. Decreased microporosity, on the other hand, renders diffusion faster and activation energies lower. Interestingly, the diffusion behavior of water into the SBA-15 framework is very similar to that in zeolites (Hong et al., 2008) at 30 °C, due to the presence of complementary micropores. The enthalpies of interaction further confirm that porous silicas with significant microporosity, such as zeolites and SBA-15, inflict great confinement to small organic molecules, as reflected in strongly exothermic interaction enthalpies. Thus, micropores may strongly confine molecules and provide both thermodynamic and kinetic

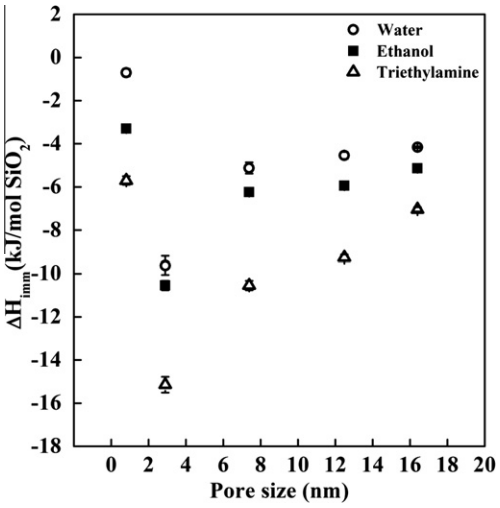

Fig. 3. Enthalpies of immersion for porous silicas per mole of SiO_2 vs. pore size in water, ethanol and triethylamine.

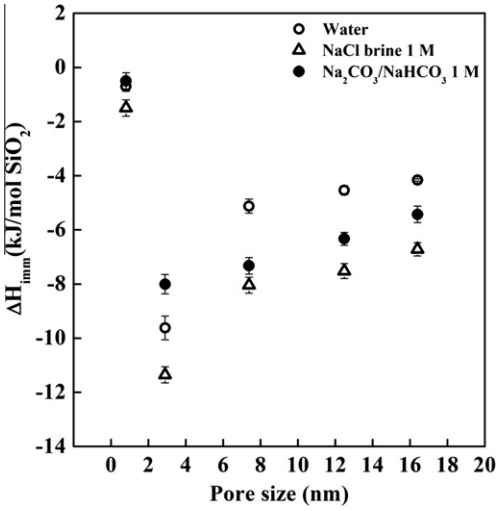

Fig. 4. Enthalpies of immersion for porous silicas per mole of SiO_2 vs. pore size in water, NaCl brine (1 M) and Na_2CO_3/$NaHCO_3$ buffer solution (1 M).

Table 2
Enthalpies of immersion (per mole of SiO_2) for porous silica samples in various liquids or solutions at 25 °C.

Sample ID	ΔH_{imm} (kJ/mol SiO2)				Na_2CO_3/$NaHCO_3$ buffer (1 M)
	Water	Ethanol	Triethylamine	NaCl brine (1 M)	
SSZ-59	−0.72 ± 0.19(7)[a]	−3.37 ± 0.18(4)	−5.74 ± 0.21(4)	−1.54 ± 0.27(5)	−0.52 ± 0.26(6)
MCM-41	−9.62 ± 0.44(6)	−10.54 ± 0.22(6)	−15.14 ± 0.36(4)	−11.35 ± 0.30(4)	−8.01 ± 0.36(5)
SBA-15_1	−5.12 ± 0.26(4)	−6.24 ± 0.09(8)	−10.55 ± 0.21(4)	−8.04 ± 0.29(6)	−7.33 ± 0.31(8)
SBA-15_2	−4.54 ± 0.16(4)	−5.94 ± 0.07(4)	−9.26 ± 0.13(4)	−7.52 ± 0.28(5)	−6.33 ± 0.24(5)
SBA-15_3	−4.15 ± 0.14(4)	−5.14 ± 0.14(4)	−7.04 ± 0.10(5)	−6.72 ± 0.25(4)	−5.43 ± 0.30(6)

[a] The value in () represents number of measurements performed.

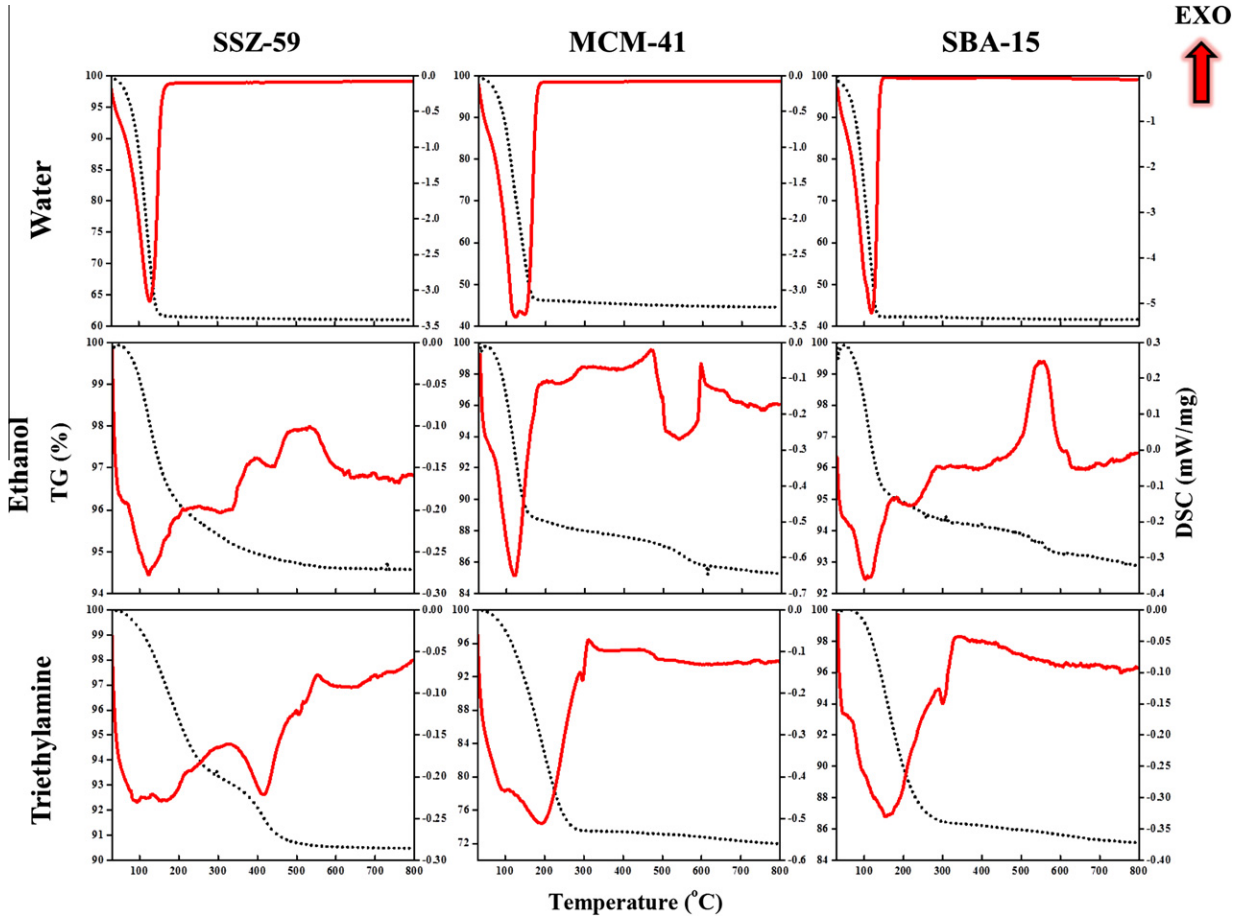

Fig. 5. TG–DSC curves (under argon at 10 °C/min) of SSZ-59, MCM-41 and SBA-15_3 after immersion calorimetry experiments with water, ethanol and triethylamine.

hindrance to their removal, even in the presence of mesopores. Such effects may be important in the geologic environment, where a broad distribution of pore sizes is expected (Burdine et al., 1950; Warren and Root, 1963; Peng et al., 2012; Tanino and Blunt, 2012).

The interaction enthalpies between porous silicas and water do not show any obvious correlation with pore size, probably due to the predominantly hydrophobic nature of pure silica surfaces (Fig. 6b). The enthalpies of interaction per mole of H_2O are weakly exothermic, and range between −0.3 and −2.3 kJ per mole of H_2O. The small absolute values of interaction enthalpies indicate that the H_2O molecules in these porous silica samples are energetically and structurally similar to bulk water, in accord with water loss near 100 °C in thermal analysis. Fig. 6b indicates that MCM-41, without microporosity, has the most exothermic enthalpy of interaction per mole of H_2O, the silica samples with micropores exhibit enthalpy of interaction values near zero. This distinct thermodynamic behavior implies that most of the H_2O molecules either stay on the surface or are very loosely confined due to limited accessibility of the micropores of SSZ-59 and SBA-15. The enthalpies confirm the generally hydrophobic nature of the silica surface. Interestingly, the hydration enthalpies of aluminosilicate zeolites were found to be −5.0 to −45.0 kJ per mole of H_2O (Sun et al., 2006). In these cases, both aluminum in the frameworks and alkali cations in the channels provide stronger interaction with H_2O, and the surfaces (internal and external) are considered to be much less hydrophobic than those of pure silica. Coupled with previous results (Sun et al., 2006; Sun and Navrotsky, 2008b; Zhou et al., 2011), the present thermodynamic data further indicate that inorganic hosts with hydrophobic pore surfaces show weak interactions with water. It is possible that the water molecules, more strongly bonded to each other than to hydrophobic surfaces, form clusters which have little thermodynamic driving force and possible steric hindrance to enter micropores. In contrast, more hydrophobic molecules (organics) may preferentially enter the micropores.

4.2. Role of surface hydroxyl groups

The interaction enthalpies of porous silicas with various liquids versus the concentration of hydroxyl groups of porous silica are plotted in Fig. 7a and b. The concentration of hydroxyl groups on the silica surface was calculated according to Mueller et al. (2003), using TG–DSC and nitrogen adsorption data and are given in Table 1. This trend is sim-

Table 3a
Weight loss (wt.%) from TG–DSC experiments (to 800 °C) of liquid absorbed/confined porous silica samples and calculated weight loss (mole) of liquid molecules per mole of porous silica.

Sample ID	Total weight loss (wt.%)			Total weight loss (mole liquid per mole SiO_2)		
	Water	Ethanol	Triethylamine	Water	Ethanol	Triethylamine
SSZ-59	38.98	4.60	9.52	2.13	0.06	0.06
MCM-41	55.45	14.14	28.03	4.15	0.22	0.23
SBA-15_1	66.29	8.54	18.84	6.56	0.12	0.14
SBA-15_2	58.35	7.09	14.88	4.68	0.10	0.10
SBA-15_3	55.67	5.93	11.03	4.19	0.08	0.07

Table 3b
Percent of total weight loss for each TGA event from TG–DSC experiments of liquid-containing porous silica samples.

Sample ID	Water		Ethanol		Triethylamine	
	TG_1 (%)	TG_2 (%)	TG_1 (%)	TG_2 (%)	TG_1 (%)	TG_2 (%)
SSZ-59	100.00 (about 100 °C)	0.00	86.52 (125 °C)	13.48 (500 °C)	64.60 (30∼300 °C)	35.40 (420 °C)
MCM-41	100.00 (about 100 °C)	0.00	75.39 (125 °C)	24.61 (500 °C)	99.50 (30∼300 °C)	0.50 (slightly above 300 °C)
SBA-15_3	100.00 (about 100 °C)	0.00	72.18 (125 °C)	27.82 (500 °C)	98.10 (30∼300 °C)	1.90 (slightly above 300 °C)

ilar to that observed in Fig. 6a and b and could be attributed to the inaccessibility of microporosity to water clusters. In the mesoporous region (MCM-41 and SBA-15), higher surface hydroxyl concentration leads to stronger adsorption/confinement for ethanol and triethylamine.

An earlier study showed that for the same SBA-15 framework, increasing hydroxyl concentration resulted in a larger amount of grafted amine, greatly enhancing the CO_2 adsorption capacity (Wang and Yang, 2011). Our results are consistent with this finding and suggest that the enthalpy of interaction of porous silicas with various polar liquids becomes more exothermic with increasing concentration of hydroxyl groups on the porous silica surface as long as the pore size is easily accessible to the guest organic molecules. The SSZ-59 framework with the lowest hydroxyl group concentration (0.8 nm^{-2}) is an exception and shows a highly exothermic interaction enthalpy with triethylamine. This may be due to a strong confinement effect of triethylamine molecules (0.78 nm) in pores (0.8 nm) only marginally larger than the molecular diameter. This interpretation is supported by the high desorption temperature of triethylamine from SSZ-59 (420 °C) observed in the TG–DSC profile compared to MCM-41 and SBA-15 (300 °C).

Hence, all the immersion calorimetric data suggest that the enthalpy of interaction of water, ethanol and triethylamine with porous silica is governed both by the framework porosity and concentration of hydroxyl groups on the porous silica surfaces. Overall, the strength of bonding under confinement increases in the order of water, ethanol and triethylamine.

4.3. Solution–porous media interactions: possible structural interpretation

The one-step weight loss of TG curves and weakly exothermic interaction enthalpies both suggest that the water confined in the porous silicas might not fill the whole pore space close to the pore walls. Instead, H_2O may only interact with the hydroxyl groups on the pore surface through hydrogen bonding, leaving cavities or gas bubbles close to the hydrophobic parts of the silica walls (Kocherbitov and Alfredsson, 2007). In other words, the confined water in porous silica frameworks may have a cluster-like structure, with only a few H_2O molecules at the "cluster" surface responsible for the overall interaction with the solid surface. This would also explain why our interaction enthalpies are lower than the values measured by gas adsorption methods (Matsumoto et al., 2001, 2002; Bolis et al., 2006). In contrast, ethanol and triethylamine may not only wet the hydrophilic sites but also the hydrophobic regions, which form the majority of the area of the silica surface, micropores, and mesopores. Results from the TG–DSC experiments with two-step desorption support this hypothesis. The detailed weight loss percentage of each TG event is listed in Table 3b. As the dimension of the guest molecule approaches the smallest pore size of a given framework, the overall energetic confinement effects from the host become stronger. As a result, a larger fraction of guest molecules is desorbed in the second (higher temperature) step of TG weight loss. The amount of triethylamine desorbed in the second step of weight loss of SSZ-59 (35.40%) and SBA-15 (1.90%) is greater than that for MCM-41 (0.50%) which only has mesoporous pores, whereas the enthalpies of interaction become less exothermic in the same sequence (see Fig. 6a). Table 5 summarizes the calculated pore – filling in terms of the percentage of solution by volume. For water-containing SSZ-59, the calculated volume of absorbed water is more than its pore volume. This may occur because, after heating at high temperature, the elimination of hydroxyl groups of the SSZ-59 framework also significantly contributes to the total amount of desorbed water. Ethanol and triethylamine molecules partially fill the pores of nanoporous silicas (see Table 5). In addition, IR measurements (not shown) confirm that ethanol and amine-containing species are absorbed directly through hydrogen

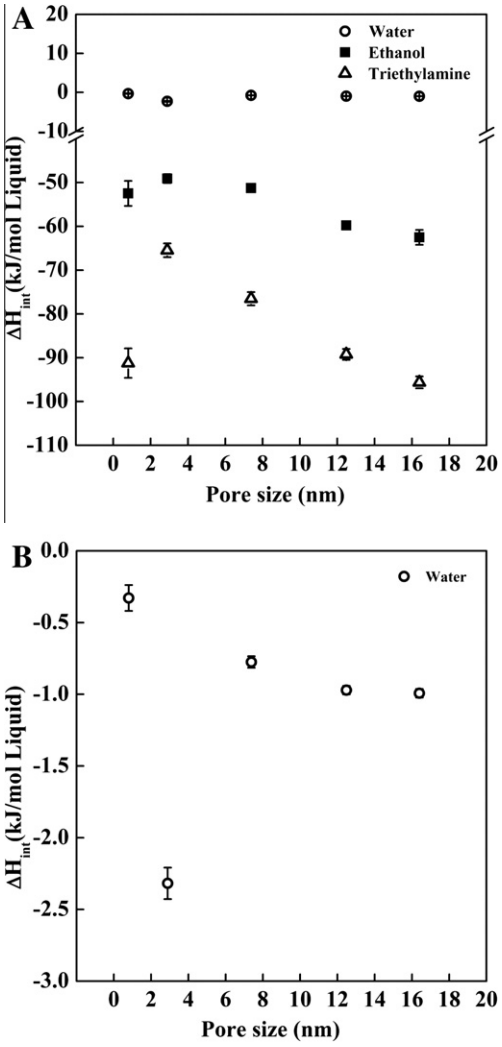

Fig. 6. (a) Enthalpies of interaction for porous silica samples per mole of liquid vs. pore size in water, ethanol and triethylamine. (b) Enthalpies of interaction for porous silica samples per mole of liquid vs. pore size in water.

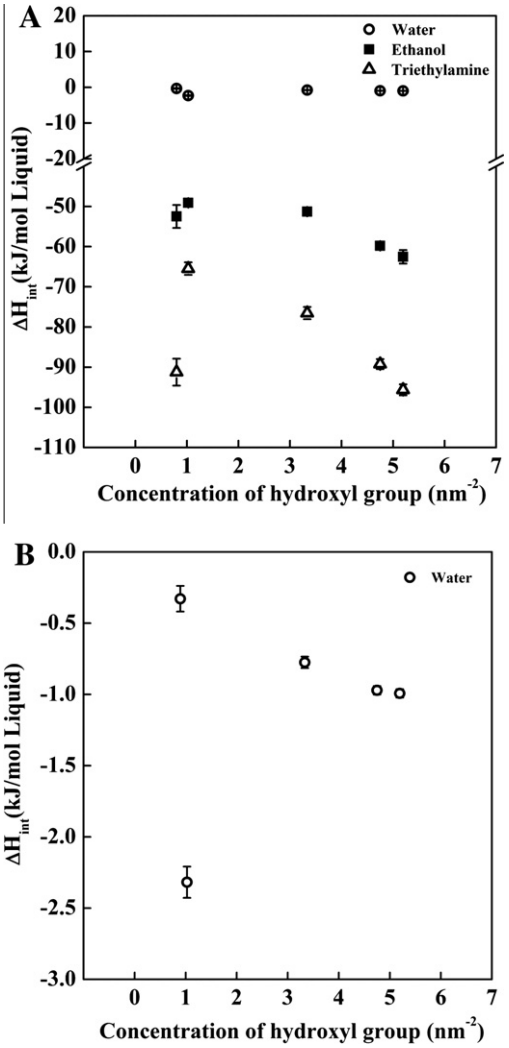

Fig. 7. (a) Enthalpies of interaction for porous silica samples per mole of liquid vs. concentration of hydroxyl group per nm^2 in water, ethanol and triethylamine. (b) Enthalpies of interaction for porous silica samples per mole of liquid vs. concentration of hydroxyl group per nm^2 in water.

Table 4
Enthalpies of interaction (per mole of absorbed/confined liquid) for porous silica samples with water, ethanol and triethylamine at 25 °C.

Sample ID	ΔH_{int} (kJ/mol solution)		
	Water	Ethanol	Triethylamine
SSZ-59	-0.33 ± 0.08	-52.48 ± 2.39	-91.24 ± 0.21
MCM-41	-2.32 ± 0.11	-49.11 ± 1.01	-65.47 ± 1.58
SBA-15_1	-0.78 ± 0.06	-51.27 ± 2.07	-76.53 ± 1.91
SBA-15_2	-0.97 ± 0.04	-59.79 ± 0.07	-89.24 ± 1.29
SBA-15_3	-0.99 ± 0.04	-62.52 ± 0.14	-95.64 ± 1.08

bonding onto the silica surfaces. Based on these observations, we propose a structural model for the interactions of water, ethanol and triethylamine with all three porous silicas, reflecting the molecular size of the guest molecules, as shown in Fig. 8. In this model, water tends to fill the pores, leaving air bubbles on the hydrophobic area, whereas ethanol and triethylamine tend to only coat the pore surfaces. These proposed structures might serve as the basis to analyze and understand guest–host interactions in geologic CO_2 sequestration and carbonate mineralization conditions. Clearly, a next step of experimentation, now in progress, is to measure the energetics of $scCO_2$ confinement as a function of pore size in the same systems.

Interestingly, quite similar phenomena have been discovered and reported by Stipp et al. (Andersson and Stipp, 2012; Bohr et al., 2010; Cooke et al., 2010; Pasarin et al., 2012; Sand et al., 2008) in their study of the molecular interaction of ethanol and/or water with the surface of calcite. They have demonstrated, both experimentally and theoretically, that ethanol molecules are able to form two types of interactions with both Ca–O and O–H functional moieties of the calcite surface to build a highly ordered, strongly

Table 5
Pore filling calculated from weight loss (wt.%) of TG–DSC experiments (800 °C) of post-immersion calorimetry porous silica samples.

Sample ID	Pore filling (% by volume)		
	Water	Ethanol	Triethylamine
SSZ-59	>100	42.86	92.86
MCM-41	95.46	34.62	75.00
SBA-15_1	50.77	8.46	20.00
SBA-15_2	30.21	4.69	10.94
SBA-15_3	22.95	3.28	6.15

*Hydroxyl groups in initial porous silica may also contribute to weight loss.

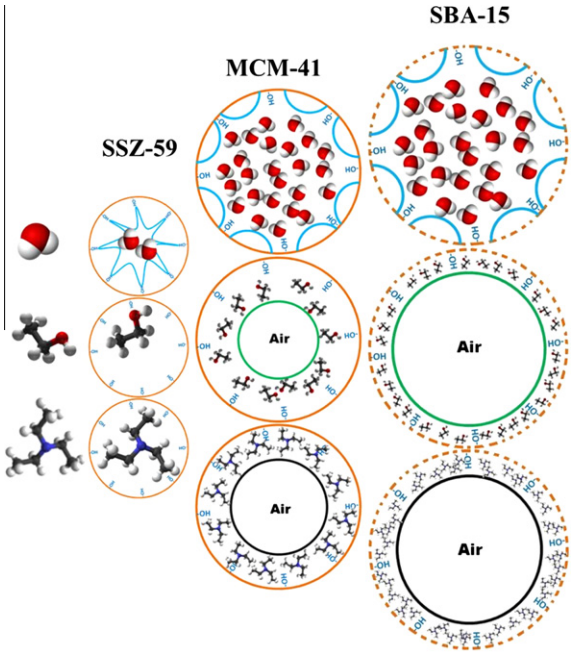

Fig. 8. Proposed structures of water (top), ethanol (middle) and triethylamine (bottom) in pores of SSZ-59 (left), MCM-41 (center) and SBA-15 (right). Dimensions are approximate.

adsorbed layered structure. Whereas, a single water molecule can only interact with one type of these sites. As a result, a less stable adsorption layer was obtained with water. The interaction of ethanol and water with the calcite surfaces is mirrored in our observations from the silica system with ethanol having muti-type stronger interactions and water showing a less strong single-type interaction with the surface. In view of this similarity between calcite and silica, analogous molecular behavior of ethanol and other organics at the mineral–fluid interface may be a more general phenomenon.

4.4. Implication for carbonate mineralization environments

Despite the significant amount of hydroxyl groups in porous silica, most of its surfaces are not hydroxylated, hence it is classified as a hydrophobic framework (Kocherbitov and Alfredsson, 2007). For subsurface carbonate mineralization and CO_2 sequestration, it is generally believed that the surfaces of caprocks sealing the reservoir are covered by strong electrolyte solutions such as brines (Liu et al., 2012). Our immersion calorimetry studies suggest that polar organic liquids bond more strongly than aqueous solutions to silica-based porous media. Therefore, for silica-rich reservoir rocks such as sandstones, organic species, especially amines, produced by subsurface organisms, the presence of petroleum, or the introduction of an impure sc-CO_2 fluid and/or contaminants from drilling may play an active role in determining the surface chemistry, especially in the availability and nature of mineral surfaces for carbonate precipitation. Organic liquids such as low molecular weight alcohols and amines have very low viscosity and surface tension, and their molecules diffuse rapidly. Their functional groups can form hydrogen bonds with silanol groups and interact with the major hydrophobic part of silica surfaces (Curthoys et al., 1974; Child et al., 1982; Kuhn et al., 2010). The adsorption of these molecules could potentially change the energetic barriers of carbonate dissolution and/or mineralization by changing silica surface properties (e.g. surface charge and hydrophibility/hydrophobility) or by helping transport and concentrate carbonate species into the limited dimensions of pore structures (Etienne and Walcarius, 2003; Huang et al., 2003; Navrotsky, 2004; Harlick and Sayari, 2007; Zelenak et al., 2008). Moreover, at the elevated temperature of subsurface geological CO_2 reservoirs (60–120 °C) and at high pressure (above 100 bars) (Diefenbacher et al., 2011), the organic guest molecules may even act as structure directing agents similar to those used in the hydrothermal/solvothermal synthesis of zeolites (Mann and Ozin, 1996; Kuhn et al., 2009; Ren et al., 2011). Such strong interactions may help determine carbonate precipitation pathways and rates, including through possible amorphous carbonate precursors.

Furthermore, a silica surface with adsorbed amine may create a favorable site for CO_2 adsorption, perhaps acting as natural functionalized CO_2 capture sorbents analogous to synthetic amines used for this purpose industrially (Zheng et al., 2005; Su et al., 2010; Mello et al., 2011; Panda et al., 2011; Yang et al., 2012), increasing the probability for carbonate species to contact and stick to the silica-rich rock surfaces, further promoting carbonate precipitation (Navrotsky, 2004). Such amine-functionalized silica surfaces may also be useful for other environmental remediation strategies, such as regulation and removal of organic or inorganic contaminants from water resources, soil and subsurface sedimental environments (Bertsch and Seaman, 1999; Aguado et al., 2009; Walcarius and Mercier, 2010; Khin et al., 2012). The measured enthalpies of immersion per mole of SiO_2 (see Table 2) indicate that the water, brine and sodium carbonate/bicarbonate buffer solutions interact weakly with the hydrophobic surface of porous silicas. Rather, more hydrophilic porous media must be sought to tailor systems that have stronger interaction with carbonate-containing aqueous solutions. Such environments could be found in clays and other aluminosilicates. Unlike silica, which has no charge-balancing cations, these negatively charged hosts associate with a wide variety of cations such as alkali and alkaline earth ions (Na^+, Mg^{2+} and Ca^{2+}) and even transition metal cations. In these cation –

exchanged, aluminum – enriched hosts, water or aqueous solutions are held more tightly than in pure silica porous materials (Sun et al., 2006, 2007; Sun and Navrotsky, 2008a). This tighter binding suggests aqueous solutions containing carbonate may bind preferentially with aluminosilicates (zeolites, clays) than with SiO_2 (quartz or amorphous silica). The adsorption of these carbonate ions may also result in further carbonate precipitation on the surfaces or in the pores of host frameworks. In rocks containing both silica and aluminosilicates, especially in the presence of organics, the chemical reactions at the surfaces may be quite different, the silica favoring CO_2 adsorption and the aluminosilicate favoring carbonate adsorption and precipitation. At these surfaces, the local pH may differ from that of the bulk brine. These phenomena deserve further careful study.

5. CONCLUSIONS

Enthalpies of immersion for calcined porous silica with different pore sizes were measured at 25 °C. Combined with TG–DSC and nitrogen adsorption data, these measurements allowed interaction enthalpies of water, ethanol and triethylamine with inorganic porous silica matrices of different pore size to be calculated. These thermochemical results suggest that amines preferentially bond to porous silica with relatively hydrophobic surfaces. Silica with smaller pores and higher surface hydroxyl group density yield stronger guest–host interactions. The role of organic interactions at silica surfaces may be important in the CO_2 sequestration environment, potentially influencing CO_2 capture and carbonate precipitation. Future thermochemical studies should be extended to other organics, including aliphatic and aromatic hydrocarbons and carboxylic acids. Studies in which both water and organic molecules compete for binding in the pores are also needed. A major point of this paper, which is a pilot study for such future work, is that relatively straightforward calorimetric measurements can provide accurate and useful information on the interaction of molecules with mineral surfaces in confined geometries.

ACKNOWLEDGMENTS

The authors thank A.V. Radha and O. Trofymluk for assistance and discussions and S.I. Zones for providing the SSZ-59 sample. This work is supported as part of the "Center of Nanoscale Control of Geologic CO_2", an Energy Frontier Research Center funded by the U.S Department of Energy, Office of Science, Office of Basic Energy Sciences under Award No. DE-AC02-05CH11231.

REFERENCES

Aguado J., Arsuaga J. M., Arencibia A., Lindo M. and Gascon V. (2009) Aqueous heavy metals removal by adsorption on amine-functionalized mesoporous silica. *J. Hazard. Mater.* **163**, 213–221.

Andersson M. P. and Stipp S. L. S. (2012) How acidic is water on calcite? *J. Phys. Chem. C* **116**, 18779–18787.

Assayag N., Matter J., Ader A., Goldberg D. and Agrinier P. (2008) CO(2) ionic trapping by water–rock interactions during a push–pull test in a basaltic–metasedimentary aquifer. *Geochim. Cosmochim. Acta* **72**, A36.

Astakhov, V. A. and Dubinin, M. M., 1971. Development of Ideas of Volume Filling of Micropores during Adsorption of Gases and Vapours by Microporous Adsorbents.3. Zeolites with Large Voids and Considerable Number of Adsorption Centers. Izvestiya Akademii Nauk Sssr-Seriya Khimicheskaya, 17-&.

Bachu S. and Stewart S. (2002) Geological sequestration of anthropogenic carbon dioxide in the western Canada sedimentary basin: suitability analysis. *J. Can. Petrol. Technol.* **41**, 32–40.

Ball P. C. and Evans R. (1989) Temperature-dependence of gas-adsorption on a mesoporous solid – capillary criticality and hysteresis. *Langmuir* **5**, 714–723.

Barrett E. P., Joyner L. G. and Halenda P. P. (1951) The determination of pore volume and area distributions in porous substances: 1. Computations from nitrogen isotherms. *J. Am. Chem. Soc.* **73**, 373–380.

Benson S. M. and Cole D. R. (2008) CO(2) sequestration in deep sedimentary formations. *Elements* **4**, 325–331.

Bertier P., Swennen R., Laenen B., Lagrou D. and Dreesen R. (2006) Experimental identification of CO_2–water–rock interactions caused by sequestration of CO_2 in Westphalian and Buntsandstein sandstones of the Campine Basin (NE-Belgium). *J. Geochem. Explor.* **89**, 10–14.

Bertsch P. M. and Seaman J. C. (1999) Characterization of complex mineral assemblages: implications for contaminant transport and environmental remediation. *Proc. Natl. Acad. Sci. U S A* **96**, 3350–3357.

Bohr J., Wogelius R. A., Morris P. M. and Stipp S. L. S. (2010) Thickness and structure of the water film deposited from vapour on calcite surfaces. *Geochim. Cosmochim. Acta* **74**, 5985–5999.

Bolis V., Busco C. and Ugliengo P. (2006) Thermodynamic study of water adsorption in high-silica zeolites. *J. Phys. Chem. B* **110**, 14849–14859.

Burdine N. T., Gournay L. S. and Reichertz P. P. (1950) Pore size distribution of petroleum reservoir rocks. *Trans. Am. Inst. Min. Metall. Eng.* **189**, 195–204.

Burton A., Elomari S., Chen C. Y., Medrud R. C., Chan I. Y., Bull L. M., Kibby C., Harris T. V., Zones S. I. and Vittoratos E. S. (2003) SSZ-53 and SSZ-59: two novel extra-large pore zeolites. *Chem. Eur. J.* **9**, 5737–5748.

Burton A., Elomari S., Chen C. Y., Harris T. V. and Vittoratos E. S. (2004) SSZ-53 and SSZ-59: two novel extra-large pore zeolites. *Stud. Surf. Sci. Catal.* **154**, 126–132.

Che S. N., Lund K., Tatsumi T., Iijima S., Joo S. H., Ryoo R. and Terasaki O. (2003) Direct observation of 3D mesoporous structure by scanning electron microscopy (SEM): SBA-15 silica and CMK-5 carbon. *Angew. Chem. Int. Ed.* **42**, 2182–2185.

Child M. J., Heywood M. J., Pulton S. K., Vicary G. A., Yong G. H. and Rochester C. H. (1982) Infrared studies of the adsorption of triethylamine on silica at the solid vapor and solid liquid interfaces. *J. Colloid Interface Sci.* **89**, 202–208.

Cole D. R., Chialvo A. A., Rother G., Vlcek L. and Cummings P. T. (2010) Supercritical fluid behavior at nanoscale interfaces: implications for CO_2 sequestration in geologic formations. *Philos. Mag.* **90**, 2339–2363.

Cooke D. J., Gray R. J., Sand K. K., Stipp S. L. S. and Elliott J. A. (2010) Interaction of Ethanol and Water with the $10(1)\bar{4}$ Surface of Calcite. *Langmuir* **26**, 14520–14529.

Corma A. (1997) From microporous to mesoporous molecular sieve materials and their use in catalysis. *Chem. Rev.* **97**, 2373–2419.

Curthoys G., Davydov V. Y., Kiselev A. V., Kiselev S. A. and Kuznetso Bv. (1974) Hydrogen-bonding in adsorption on silica. *J. Colloid Interface Sci.* **48**, 58–72.

deCarvalho M. B., Pires J. and Carvalho A. P. (1996) Characterisation of clays and aluminium pillared clays by adsorption of probe molecules. *Microporous Mater.* **6**, 65–77.

Diefenbacher J., Piwowarczyk J. and Marzke R. F. (2011) Note: Solution NMR probe for the study of CO_2 sequestration at elevated pressure and temperature. *Rev. Sci. Instrum.* **82**, 076107.

Dove P. M., De Yoreo J., Weiner S. and Mineralogical Society of America (2003) *Biomineralization*. Mineralogical Society of America, Washington, DC.

Etienne M. and Walcarius A. (2003) Analytical investigation of the chemical reactivity and stability of aminopropyl-grafted silica in aqueous medium. *Talanta* **59**, 1173–1188.

Fusco S., Borzacchiello A. and Netti P. A. (2006) Perspectives on: PEO–PPO–PEO triblock copolymers and their biomedical applications. *J. Bioact. Compat. Polym.* **21**, 149–164.

Galarneau A., Cambon N., Di Renzo F., Ryoo R., Choi M. and Fajula F. (2003) Microporosity and connections between pores in SBA-15 mesostructured silicas as a function of the temperature of synthesis. *New J. Chem.* **27**, 73–79.

Gallis K. W. and Landry C. C. (1997) Synthesis of MCM-48 by a phase transformation process. *Chem. Mater.* **9**, 2035–2038.

Glinka C. J., Nicol J. M., Stucky G. D., Ramli E., Margolese D., Huo Q., Higgins J. B. and Leonowicz M. E. (1996) Small angle neutron scattering study of the structure and formation of MCM-41 mesoporous molecular sieves. *J. Porous Mater.* **3**, 93–98.

Harlick P. J. E. and Sayari A. (2007) Applications of pore-expanded mesoporous silica: 5. Triamine grafted material with exceptional CO(2) dynamic and equilibrium adsorption performance. *Ind. Eng. Chem. Res.* **46**, 446–458.

Hoang V. T., Huang Q. L., Eic M., Do T. O. and Kaliaguine S. (2005) Structure and diffusion characterization of SBA-15 materials. *Langmuir* **21**, 2051–2057.

Hong C. K., Lee J., Jang Y. B., Kim T. H., Yeo J. G., Ahn Y. S. and Cho S. J. (2008) Adsorption of water on mesoporous silica for heat management: effect of pore structure. *J. Nanosci. Nanotechnol.* **8**, 5471–5474.

Huang H. Y., Yang R. T., Chinn D. and Munson C. L. (2003) Amine-grafted MCM-48 and silica xerogel as superior sorbents for acidic gas removal from natural gas. *Ind. Eng. Chem. Res.* **42**, 2427–2433.

Joyner L. G., Barrett E. P. and Skold R. (1951) The determination of pore volume and area distributions in porous substances: 2. Comparison between nitrogen isotherm and mercury porosimeter methods. *J. Am. Chem. Soc.* **73**, 3155–3158.

Kharaka Y. K., Cole D. R., Hovorka S. D., Gunter W. D., Knauss K. G. and Freifeld B. M. (2006a) Gas-water-rock interactions in Frio Formation following CO_2 injection: implications for the storage of greenhouse gases in sedimentary basins. *Geology* **34**, 577–580.

Kharaka Y. K., Cole D. R., Thordsen J. J., Kakouros E. and Nance H. S. (2006b) Gas–water–rock interactions in sedimentary basins: CO_2 sequestration in the Frio Formation, Texas, USA. *J. Geochem. Explor.* **89**, 183–186.

Khin M. M., Nair A. S., Babu V. J., Murugan R. and Ramakrishna S. (2012) A review on nanomaterials for environmental remediation. *Energy Environ. Sci.* **5**, 8075–8109.

Kocherbitov V. and Alfredsson V. (2007) Hydration of MCM-41 studied by sorption calorimetry. *J. Phys. Chem. C* **111**, 12906–12913.

Kruk M., Jaroniec M., Ko C. H. and Ryoo R. (2000) Characterization of the porous structure of SBA-15. *Chem. Mater.* **12**, 1961–1968.

Kuhn J., Castillo-Sanchez J. M., Gascon J., Calero S., Dubbeldam D., Vlugt T. J. H., Kapteijn F. and Gross J. (2009) Adsorption and diffusion of water, methanol, and ethanol in all-silica DD3R: experiments and simulation. *J. Phys. Chem. C* **113**, 14290–14301.

Kuhn J., Castillo-Sanchez J. M., Gascon J., Calero S., Dubbeldam D., Vlugt T. J. H., Kapteijn F. and Gross J. (2010) Adsorption and diffusion of water, methanol, and ethanol in all-silica DD3R: experiments and simulations (vol 113C, pg 14290, 2009). *J. Phys. Chem. C* **114**, 6877–6878.

Lalik E., Mirek R., Rakoczy J. and Groszek A. (2006) Microcalorimetric study of sorption of water and ethanol in zeolites 3A and 5A. *Catal. Today* **114**, 242–247.

Li Z. W., Dong M. Z., Li S. L. and Huang S. (2006) CO_2 sequestration in depleted oil and gas reservoirs – caprock characterization and storage capacity. *Energy Convers. Manage.* **47**, 1372–1382.

Liu F. Y., Lu P., Griffith C., Hedges S. W., Soong Y., Hellevang H. and Zhu C. (2012) CO_2–brine–caprock interaction: reactivity experiments on Eau Claire shale and a review of relevant literature. *Int. J. Greenhouse Gas Control* **7**, 153–167.

Mann S. and Ozin G. A. (1996) Synthesis of inorganic materials with complex form. *Nature* **382**, 313–318.

Marini L. (2007) *Geological Sequestration of Carbon dioxide: Thermodynamics, Kinetics, and Reaction Path Modeling*. Elsevier, Amsterdam, Boston.

Matsumoto A., Sasaki T., Nishimiya N. and Tsutsumi K. (2001) Evaluation of the hydrophobic properties of mesoporous FSM-16 by means of adsorption calorimetry. *Langmuir* **17**, 47–51.

Matsumoto A., Tsutsumi K., Schumacher K. and Unger K. K. (2002) Surface functionalization and stabilization of mesoporous silica spheres by silanization and their adsorption characteristics. *Langmuir* **18**, 4014–4019.

Mello M. R., Phanon D., Silveira G. Q., Llewellyn P. L. and Ronconi C. M. (2011) Amine-modified MCM-41 mesoporous silica for carbon dioxide capture. *Microporous Mesoporous Mater.* **143**, 174–179.

Mueller R., Kammler H. K., Wegner K. and Pratsinis S. E. (2003) OH surface density of SiO_2 and TiO_2 by thermogravimetric analysis. *Langmuir* **19**, 160–165.

Navrotsky A. (2004) Energetic clues to pathways to biomineralization: precursors, clusters, and nanoparticles. *Proc. Natl. Acad. Sci. U S A* **101**, 12096–12101.

Panda T., Pachfule P., Chen Y. F., Jiang J. W. and Banerjee R. (2011) Amino functionalized zeolitic tetrazolate framework (ZTF) with high capacity for storage of carbon dioxide. *Chem. Commun.* **47**, 2011–2013.

Pasarin I. S., Yang M., Bovet N., Glyvradal M., Nielsen M. M., Bohr J., Feidenhans'l R. and Stipp S. L. S. (2012) Molecular Ordering of Ethanol at the Calcite Surface. *Langmuir* **28**, 2545–2550.

Peng S., Hu Q. H. and Hamamoto S. (2012) Diffusivity of rocks: gas diffusion measurements and correlation to porosity and pore size distribution. *Water Resour. Res.* **48**.

Piccione P. M., Yang S. Y., Navrotsky A. and Davis M. E. (2002) Thermodynamics of pure-silica molecular sieve synthesis (vol 106B, pg 3629, 2002). *J. Phys. Chem. B* **106**, 5312.

Pollock R. A., Walsh B. R., Fry J., Ghampson I. T., Melnichenko Y. B., Kaiser H., Pynn R., DeSisto W. J., Wheeler M. C. and Frederick B. G. (2011) Size and spatial distribution of micropores in SBA-15 using CM-SANS. *Chem. Mater.* **23**, 3828–3840.

Rathousky J., Zukal A., Franke O. and Schulzekloff G. (1994) Adsorption on Mcm-41 mesoporous molecular-sieves: 1. Nitrogen isotherms and parameters of the porous structure. *J. Chem. Soc., Faraday Trans.* **90**, 2821–2826.

Ren D. N., Feng Q. L. and Bourrat X. (2011) Effects of additives and templates on calcium carbonate mineralization in vitro. *Micron* **42**, 228–245.

Ruthven D. M. (2011) Molecular sieve separations. *Chem. Ing. Tech.* **83**, 44–52.

Ryoo R., Ko C. H., Kruk M., Antochshuk V. and Jaroniec M. (2000) Block-copolymer-templated ordered mesoporous silica: array of uniform mesopores or mesopore–micropore network? *J. Phys. Chem. B* **104**, 11465–11471.

Sand K. K., Stipp S. L. S., Hassenkam T., Yang M., Cooke D. and Makovicky E. (2008) Ethanol adsorption on the 10(1)$\bar{4}$ calcite surface: preliminary observations with atomic force microscopy. *Mineral Mag* **72**, 353–357.

Schnaar G. and Digiulio D. C. (2009) Computational modeling of the geologic sequestration of carbon dioxide. *Vadose Zone J.* **8**, 389–403.

Su F. S., Lu C. Y., Kuo S. C. and Zeng W. T. (2010) Adsorption of CO_2 on amine-functionalized Y-type zeolites. *Energy Fuel* **24**, 1441–1448.

Sun P. P. and Navrotsky A. (2008a) Enthalpy of formation and dehydration of alkaline earth cation exchanged zeolite beta. *Microporous Mesoporous Mater.* **109**, 147–155.

Sun P. P. and Navrotsky A. (2008b) Formation and dehydration enthalpy of gallosilicate zeolites. *Microporous Mesoporous Mater.* **111**, 507–516.

Sun P. P., Deore S. and Navrotsky A. (2006) Formation and dehydration enthalpy of ion exchanged zeolite beta. *Microporous Mesoporous Mater.* **91**, 15–22.

Sun P. P., Deore S. and Navrotsky A. (2007) Enthalpy of formation and dehydration of lithium and sodium zeolite beta. *Microporous Mesoporous Mater.* **98**, 29–40.

Tanino Y. and Blunt M. J. (2012) Capillary trapping in sandstones and carbonates: dependence on pore structure. *Water Resour. Res.* **48**, W12529.

Trofymluk O., Levchenko A. A., Tolbert S. H. and Navrotsky A. (2005) Energetics of mesoporous silica: investigation into pore size and symmetry. *Chem. Mater.* **17**, 3772–3783.

Trofymluk O., Levchenko A. A. and Navrotsky A. (2012) Mesoporous silica synthesis: energetics of interaction between framework and structure directing agent. *Microporous Mesoporous Mater.* **149**, 119–125.

Walcarius A. and Mercier L. (2010) Mesoporous organosilica adsorbents: nanoengineered materials for removal of organic and inorganic pollutants. *J. Mater. Chem.* **20**, 4478–4511.

Wang L. F. and Yang R. T. (2011) Increasing selective CO(2) adsorption on amine-grafted SBA-15 by increasing silanol density. *J. Phys. Chem. C* **115**, 21264–21272.

Warren J. E. and Root P. J. (1963) The behavior of naturally fractured reservoirs. *Soc. Petrol. Eng. J.* **3**, 245–255.

Weiner S. and Dove P. M. (2003) An overview of biomineralization processes and the problem of the vital effect. *Biomineralization* **54**, 1–29.

Wurdemann H., Moller F., Kuhn M., Heidug W., Christensen N. P., Borm G., Schilling F. R. and Grp C. s. (2010) CO2SINK-from site characterisation and risk assessment to monitoring and verification: one year of operational experience with the field laboratory for CO_2 storage at Ketzin, Germany. *Int. J. Greenhouse Gas Control* **4**, 938–951.

Yang S. T., Kim J. Y., Kim J. and Ahn W. S. (2012) CO_2 capture over amine-functionalized MCM-22, MCM-36 and ITQ-2. *Fuel* **97**, 435–442.

Zelenak V., Halamova D., Gaberova L., Bloch E. and Llewellyn P. (2008) Amine-modified SBA-12 mesoporous silica for carbon dioxide capture: effect of amine basicity on sorption properties. *Microporous Mesoporous Mater.* **116**, 358–364.

Zhao D. Y., Huo Q. S., Feng J. L., Chmelka B. F. and Stucky G. D. (1998) Nonionic triblock and star diblock copolymer and oligomeric surfactant syntheses of highly ordered, hydrothermally stable, mesoporous silica structures. *J. Am. Chem. Soc.* **120**, 6024–6036.

Zheng F., Tran D. N., Busche B. J., Fryxell G. E., Addleman R. S., Zemanian T. S. and Aardahl C. L. (2005) Ethylenediamine-modified SBA-15 as regenerable CO_2 sorbent. *Ind. Eng. Chem. Res.* **44**, 3099–3105.

Zhou W., Sun P. P., Zhang P. and Navrotsky A. (2011) Thermochemistry of proton containing borosilicate, aluminosilicate and gallosilicate zeolite beta. *Microporous Mesoporous Mater.* **142**, 749–753.

Associate editor: Alfonso Mucci